High-resolution angle-resolved photoemission spectroscopy study of monolayer and bilayer graphene on the C-face of SiC

E. Moreau, S. Godey, X. Wallart, I. Razado-Colambo, J. Avila, M.C. Asensio, D. Vignaud

High-resolution angle-resolved photoemission spectroscopy study of monolayer and bilayer graphene on the C-face of SiC

E. Moreau,[1] S. Godey,[1] X. Wallart,[1] I. Razado-Colambo,[1,2] J. Avila,[2] M.-C. Asensio,[2] and D. Vignaud[1,*]

[1]*IEMN, UMR CNRS 8520, Av. Poincaré, P. O. Box 60069, 59652 Villeneuve d'Ascq Cedex, France*

[2]*Synchrotron SOLEIL, L'Orme des Merisiers, Saint-Aubin P. O. Box 48, 91192 Gif sur Yvette Cedex, France*

(Received 13 February 2013; revised manuscript received 1 July 2013; published 7 August 2013)

High-energy and k-space resolution angle-resolved photoemission spectroscopy experiments were achieved on nominally single and bilayer graphene grown by Si-flux assisted molecular beam epitaxy (MBE) on the C-face of SiC. This material shows the same structure as the graphene grown by standard high-temperature annealing of SiC, noticeably the rotational disorder and the very weak electronic coupling between stacked layers. The SiC substrate induces a strong doping by charge transfer, with a Dirac point located 320 meV below the Fermi level for monolayer graphene. The efficient screening by the successive graphene layers results in a reduction of this value to 190 meV for bilayer graphene. The opening of an energy band gap, whose width is inversely dependent on the thickness, is also reported. These measurements emphasize the potentialities of the Si-flux assisted MBE technique, more particularly for homogeneous low thickness graphene growth on the C-face of SiC.

DOI: 10.1103/PhysRevB.88.075406 PACS number(s): 73.22.Pr, 81.05.ue, 61.48.Gh, 68.65.Pq

The generation of a C-rich thin layer resulting from Si sublimation during high-temperature annealing of SiC had been known for decades, even before this layer was called graphene.[1] Studies of the graphene on SiC electronic transport properties began in 2004 and became a hot topic as soon as it was realized that graphitization could be the first technique of graphene production compatible with standard technological processes for making electronic devices and able to make use of the graphene high mobilities.[2,3] SiC is a polar semiconductor, which means that it is terminated by a Si-rich surface on one side, the so-called (0001) face, and is C-rich on the rear one, labeled (000-1). The main characteristics of the graphene resulting from high-temperature annealing (the graphitization process) are strongly face-dependent.[4] In short, on the Si-face, the growth rate is slow and saturates, a $(6\sqrt{3}\times 6\sqrt{3})\mathrm{R}30^\circ$ reconstructed layer stands at the interface,[5] and the stacking of few layers is identical to the graphite one (referred to as Bernal or AB stacking). On the contrary, the growth rate remains high on the C-face without any interfacial layer[5,6] and with a very peculiar stacking of multiple layers which involves rotational disorder and results in such thick films to behave almost as a stack of electronically uncoupled single layers.[7,8] If initial experiments had been achieved under ultrahigh vacuum (UHV) conditions, it was demonstrated that the graphitization temperature range would depend on the experimental conditions and noticeably on the pressure.[9,10] The reduction and the control of the Si sublimation induced by high-pressure conditions seems to be key for obtaining high-quality material at graphitization temperatures higher than under UHV conditions.[10] If graphene on SiC has been mainly obtained by graphitization, molecular beam epitaxy (MBE)[11–13] as well as chemical vapor deposition (CVD)[14,15] were also studied. Despite the very different growth process involved (annealing only for graphitization on one side, MBE or CVD on the other side), an identical SiC face-dependency of the graphene structure is observed.

A typical characteristic of the graphene electronic-band structure is the linear dispersion of the π and π^* bands, which cross each other at the Dirac K and K′ points.[16] For undoped graphene, the Fermi-level E_F equals the Dirac point energy E_D. The interface structure on (0001) SiC and the charge transfer from the substrate induce an n-type doping of graphene.[17] The energy difference $E_F - E_D$ (which is >0 for n-type doping) is a measure of the doping, since the total density of occupied states in this 2D system is proportional to the square of this difference.[16] Angle-resolved photoemission spectroscopy (ARPES) experiments for graphene on (0001) SiC show the linear π-valence bands, with E_F standing 400–450 meV above E_D for one monolayer (ML) graphene thickness.[18–22] No clear conclusion can be reached from similar ARPES experiments achieved on (000-1) SiC. Very limited doping was most often reported, either p type with $E_F - E_D = -15$ meV for a 3–10 ML-thick sample[23] or a variable from p type (-33 meV) to n type (14 meV) for 11–12 ML graphene[24] or lower than 50 meV (respectively 75 meV) for 3 (2) ML.[25] On the contrary, larger values were measured after k-resolved photoemission electron microscopy, 0.3 eV (respectively 0.25 eV) for 2 ML (3 ML).[26] From interband differential spectroscopic measurements, it was concluded that E_D respectively stands 360, 215, 140, and 93 meV below E_F for the four graphene layers closer to the SiC substrate.[27] From scanning tunneling spectroscopy experiments, n-type doping (125 mV) was measured for an estimated thickness of 6 ML[28] and p type (-30 meV) for a thicker 10 ML sample.[29] Electrostatic screening may explain the thickness dependency of these measurements[30] because of the short screening length perpendicular to the graphene plane.[31] This is fully consistent with low-doping values at large graphene thickness. In fact, fitting their experimental charge density results with an exponential law, it was shown in Ref. 27 that the charge density is reduced by a factor of $\sim$100 above 6 ML, equivalent to a 10 times reduction of the difference $E_F - E_D$ compared to the 1 ML case. The residual low doping at large thicknesses may result from extrinsic[32,33] or intrinsic origin;[17] however, important discrepancies between the published results remain, particularly at low graphene thickness ($\leqslant$3 ML). We suggest that they may originate from the difficulty to grow sufficiently homogeneous ML-thick graphene on the C face of SiC by

graphitization,[34,35] probably because of the high growth rate that occurs whatever the experimental conditions. The purpose of this work is to present ARPES measurements on low thickness graphene (∼1 and 2 ML) grown by MBE on (000-1) SiC. A clear thickness-dependent *n*-type doping is observed, emphasizing the potentialities of the MBE technique to grow such a thin layer of graphene.

Graphene samples were grown on *n*-type 4H:SiC (000-1). The details of the UHV MBE growth set-up and conditions were already published.[12,13,36] In short, after ∼900 °C degassing, *in situ* surface flattening was performed at 1050–1100 °C under a moderate Si flux.[37] The temperature was then increased to the desired growth temperature (typically up to 1180 °C). Si sublimation and thus graphitization were prevented by simultaneously increasing the Si flux (Si-flux assisted MBE), which was checked by *in situ* monitoring of the reflected high-energy electron diffraction pattern. After stabilization of the sample temperature and Si flux, growth from a high temperature carbon solid cell was achieved. Once cooled down, low-energy electron diffraction (LEED) pattern and Auger spectroscopy measurements were recorded in another UHV-connected chamber. Angle-resolved x-ray photoemission spectroscopy (XPS) measurements were achieved after transfer at atmospheric pressure to a separate chamber [see Fig. 1(a)]. The graphene thickness was calculated from the angular dependency of the integrated intensity ratio of the graphene and substrate C1s components [Fig. 1(b)].[12,36,38] Two samples grown on SiC (000-1) are detailed here, with a nominal coverage of ML and bilayer graphene. One sample with a similar bilayer coverage was also grown on 6H:SiC (0001) using the same Si-flux assisted MBE technique for comparison purposes. The surface topography was studied by atomic force microscopy (AFM) in tapping mode.[39] ARPES experiments were then achieved at the ANTARES beam line of the SOLEIL synchrotron, with the combined instrumental energy resolution of ∼10 meV and momentum resolution of ±0.005 Å^{-1}. After atmospheric pressure transfer, samples were first systematically annealed for at least 2 hours in the 900–950 °C temperature range to avoid any residual surface contamination, often responsible for a *p*-type doping of graphene.[33] The valence band dispersion was then measured at ∼100 K using either 100 eV (linearly polarized) or 30 eV (circularly polarized) light (beam diameter ∼ 40 μm), with a Scienta R4000 detector aligned along the ΓK graphene direction. This set of measurement conditions was used in order to detect both branches of the π and π^* bands at the same time, from which the Dirac energy E_D could be deduced as their intersection point. It is known that along the ΓK direction, only one branch for each of the π and π^* bands are observable with linear polarization, due to matrix element effects,[40] while all branches are measurable for circular polarization under a limited energy range.[22,41] Perpendicular to the ΓK direction, both branches are observed under linear polarization. The orientation of the detector implies successive azimuthal recordings to obtain a full 3D measurement (vs energy, polar, and azimuthal angles) with sufficient precision. Furthermore, the identification of the Dirac point position may be hard to achieve perpendicular to the ΓK direction because of the continuous distribution of graphene orientation. This is why all the ARPES measurements presented in the following were obtained for graphene domains oriented along the SiC [11-20] direction (see Fig. 2).

The LEED patterns recorded for the MBE graphene samples are respectively shown in Figs. 2(a) (ML) and 2(b) (bilayer). Both show the typical feature for the rotationally disordered graphene on SiC (000-1), which is a distribution of graphene orientations with an intense spot along the ⟨11-20⟩ SiC directions and less intense arcs approximately located at ±(3 to 11°) on both sides from the ⟨10-10⟩ directions.[4] The SiC (3 × 3) surface reconstruction spots are dominant on the ML pattern and appear as weak traces for the bilayer sample. Although its atomic structure is not known, this reconstruction is always observed at the onset of graphitization on (000-1) SiC[42] as well as by MBE.[13] The constant energy map at the Dirac point measured for the bilayer sample is shown in Fig. 2(c). There is a clear similarity between the graphene ARPES and LEED patterns, which illustrates the graphene orientation distribution. The LEED pattern characteristics of Si-flux assisted MBE graphene are identical to the already published ones for annealed-only graphene.[4] It is important to point out that although both techniques result in the same structure, they completely differ in the involved mechanisms. MBE growth occurs at the surface, while graphitization is an interface process that involves a strong atomic reorganization induced by the migration/sublimation of the Si atoms. The

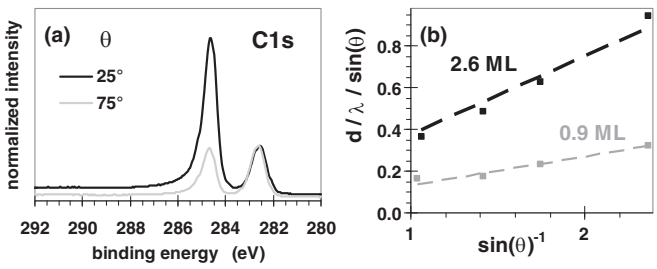

FIG. 1. (a) XPS spectra C1s component recorded for the bilayer graphene sample vs the photoemitted electron angle θ (measured relative to the sample surface) and normalized to the 282.6 eV Si-C peak intensity, and (b) fit of the angular-dependency of the 284.6 eV C-C and Si-C peak ratio to obtain the graphene thickness d (λ stands for the photoemitted electron escapelength).

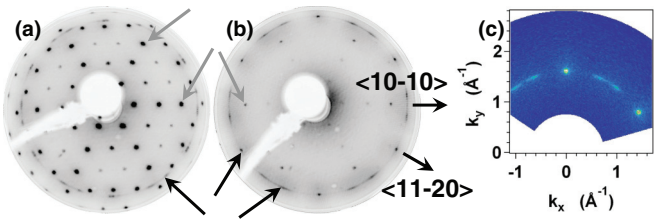

FIG. 2. (Color online) 75 V LEED pattern for nominally (a) single- or (b) bilayer-thick MBE graphene grown at 1180 °C on the C face of SiC and ARPES constant energy map at the Dirac point for the bilayer sample (for $h\nu = 100$ eV) (c). The crystallographic directions, identical for the three figures, correspond to the SiC reciprocal lattice. The (1 × 1) (gray arrows) and (3 × 3) SiC surface reconstruction spots are only observed on the LEED patterns. The graphene spots and arcs are identically observed for both LEED (black arrows) and ARPES.

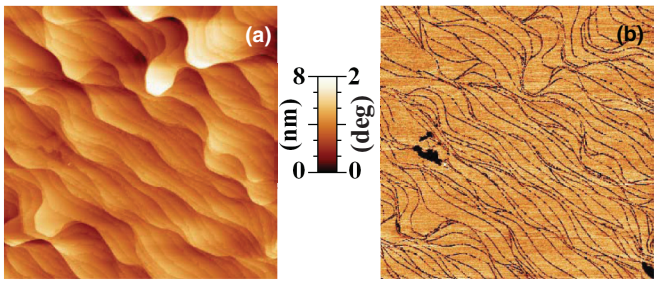

FIG. 3. (Color online) 10×10 μm^2 atomic force microscopy topographic (a) and phase (b) images of nominally monolayer-MBE graphene, grown at 1180 °C on the C face of SiC.

ML sample surface topographic and phase images obtained by AFM are shown in Fig. 3. Noticeably, apart from the topographic contrast induced by the steps, the tapping-mode phase image in Fig. 3(b) shows a rather homogeneous and constant signal, except for a few domains where the different phase shows that a material, which is not graphene, is present on the surface.[43] The analogy with the observations made at the onset of graphitization on SiC (000-1)[39] suggests that the bright areas correspond to graphene while the darker one comes from some SiC bare material domains. This point is furthermore qualitatively supported by its consistency with the graphene thickness, as determined after XPS measurements (0.9 ML). If one assumes that the substrate surface is covered either by 1 ML of graphene or by the bare SiC, the bright areas should represent 90% of the total surface which is approximately the case.

The valence band dispersion of the bilayer sample on SiC (000-1) is shown in Figs. 4(a) and 4(b), respectively, perpendicular and parallel to the ΓK direction [see the graphene Brillouin zone schematized in Fig. 4(d)]. One single graphene-domain orientation, leading to spots along the [11-20] SiC direction [see LEED pattern in Fig. 2(b)], has been selected for all the measurements presented in Fig. 4. As expected because of the respective choice of photon energy and polarization, the two branches of the π band are clearly observed in both cases. The filled squares in Fig. 4(a) are the k-space positions of the experimental intensity maxima plotted as a function of energy [for clarity, these maxima are only shown in Fig. 4(a)]. The valence band maximum energy E_{VBM} is found 215 meV below the Fermi level, which implies n-type doping in this sample. The slope of the $E(k)$ distribution is proportional to the Fermi velocity. The experimental measurements are gathered in Table I. Almost equal Fermi velocities of 1.09×10^6 and 1.08×10^6 m/s are obtained for both branches of the π band perpendicular to the ΓK direction [Fig. 4(a)]. They are identical within experimental errors to the ones already determined for equivalent[26] or thicker graphitized material on SiC (000-1),[24] on SiC (0001),[21] and for mechanically exfoliated ML graphene.[44] The valence band dispersion measured along the ΓK direction is shown in Fig. 4(b). It leads to a position of the Dirac energy, identical within experimental errors to the one shown in Fig. 4(a). ARPES experiments (not shown) on the same sample but for graphene aligned close to the [10-10] directions [see Fig. 2(b)] lead to a similar conclusion. The slopes of both branches of the π band, and thus the Fermi velocities, are slightly asymmetric along the ΓK direction: $v_{F+} = 1.14 \times 10^6$ m/s and $v_{F-} = 0.94 \times 10^6$ m/s, where v_{F+} (respectively v_{F-}) corresponds to the branch with positive (negative) slope dE/dk (see Table I). The v_{F-} branch along the ΓK direction is the one associated with the dark corridor in linear polarization ARPES experiments, as stated by Gierz *et al.*[22] This intensity asymmetry was shown to be a manifestation of the electronic chirality.[40,45] The slope asymmetry, which appears as isoenergy curves with noncircular shapes, is energy dependent and is induced by trigonal warping of the band structure in graphene.[45] Our findings are consistent with the ARPES data reported for graphitized graphene on SiC, either on the Si-[22] or on the C-face.[41] This observation points that the Si-assisted MBE growth technique is able to produce thin graphene on (000-1) SiC with the expected band structure.

The band dispersion measured by ARPES with the nominally ML sample is shown in Fig. 5(a) for graphene domains oriented along the SiC [11-20] direction. One obtains $E_F - E_{\mathrm{VBM}} \sim 420$ meV. Therefore, this ML is n-type doped similar to the bilayer case. The measured Fermi velocities are again asymmetric for the π band, with $v_{F+} = 1.14 \times 10^6$ m/s and $v_{F-} = 1.00 \times 10^6$ m/s (see Table I).

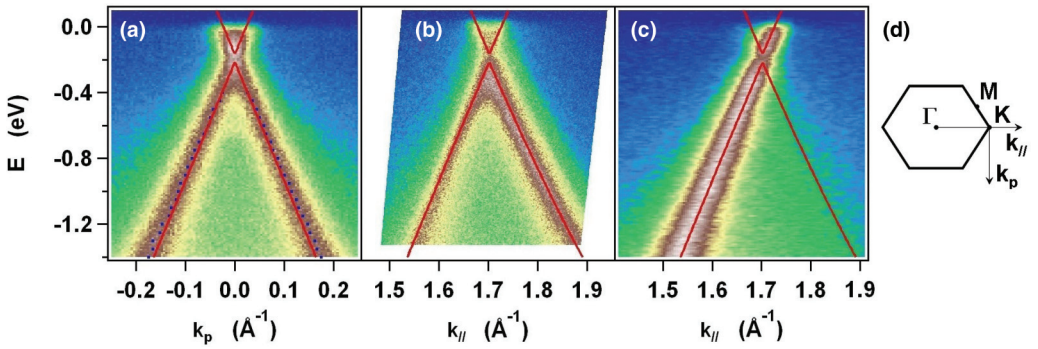

FIG. 4. (Color online) The valence band dispersion measured by ARPES perpendicular to the ΓK direction [(a) $h\nu = 100$ eV, linear polarization] or parallel to it [(b) $h\nu = 30$ eV, circular polarization and (c) $h\nu = 100$ eV, linear polarization] for bilayer MBE graphene grown at 1180 °C on the C face of SiC for graphene domains oriented along the [11-20] SiC direction. The squares (a) are the measured intensity maxima, and the continuous lines (a, b, c) are the tight-binding best fits. The Fermi level is taken as energy reference. The graphene single domain Brillouin zone scheme is shown in (d).

TABLE I. Main characteristics of the samples and corresponding valence band ARPES measurements, XPS-determined thickness, direction of ARPES measurements, Fermi velocities v_{F+} and v_{F-}, valence band maximum and Dirac energies relative to the Fermi level and corresponding figure.

Thickness (ML)	Direction	v_{F+} (m/s)	v_{F-} (m/s)	$E_F - E_{VBM}$ (meV)	$E_F - E_D$ (meV)	Figure
2.6	$\perp \Gamma K$	1.09×10^6	1.08×10^6	215	190	4(a)
	ΓK	1.14×10^6	9.37×10^5			4(b)
0.9	ΓK	1.14×10^6	9.98×10^5	420	320	5(a)

The valence band dispersion of the bilayer sample shown in Fig. 4 only shows one π band. Because the doping differs between the first and second layer (that is, compare the E_{VBM} values in Table I, see also Figs. 4 and 5), one would expect to observe two bands in the bilayer ARPES spectra. Using the E_{VBM} energy difference of 205 meV (see Table I) and an average slope of 1.1 10^6 m/s, the calculated band separation is 0.027 Å^{-1}. This is well below the measured full width at half-maximum of the momentum distribution curves, which stands in the range 0.05–0.07 Å^{-1}. The overlap between the valence bands associated with the first and second layers thus prevents us to observe two separated bands. The rotational disorder between the stacked graphene layers probably contributes to the k broadening of the bands.

Similar ARPES experiments were achieved on another nominally bilayer sample, also grown by Si-flux assisted MBE but on the Si-face of SiC. Graphene is dominant on the LEED pattern (not shown), and the standard $(6\sqrt{3} \times 6\sqrt{3})$R30° interface reconstruction[5] is also observed, although attenuated by the surface graphene. The XPS-measured graphene thickness is 2.5 ML, and its valence band dispersion is shown in Fig. 6(a) (at 30 eV with circularly polarized light), together with the momentum distribution curves taken at −1.1 eV [Fig. 6(b)]. The valence band curves are very similar to the ones measured on ∼2-ML-thick graphitized graphene on (0001) SiC,[18,19,21] in terms of the number of π bands [2, see intensity profile in Fig. 6(b)] and of the position of the extremum of the π and π^* bands, ∼250 to 400 meV below the Fermi level. Let us mention that the experimental k separation of both bands is ∼0.07 Å^{-1} for a graphene bilayer on (0001) SiC [see the momentum distribution curve in Fig. 6(b)], well above the expected one for a graphene bilayer on (000-1) SiC (∼0.027 Å^{-1}). This is why separated bands are observed in the former case but not in the latter. This observation means that the Si-flux assisted MBE technique does not significantly alter either the structure or the doping of the graphene grown on the SiC Si-face, which in turn suggests that this conclusion also holds for graphene on the other C-face. Thus, the low-thickness dependence of the doping for graphene on (000-1) SiC is a real effect resulting from the very efficient electrostatic screening induced by the successive graphene layers.[30]

The continuous lines shown in Figs. 4–6 are the best fits of the ARPES measurements using the tight-binding calculated dispersion of the graphene π and π^* bands.[31] In the case of the bilayer sample on the C-face of SiC, the almost uncoupled behavior of the two layers is shown by the valence band linear distribution close to the Dirac point: this justifies the use of the tight-binding graphene ML equations.[31] Fitting the ARPES 30 eV measurements alone lacks accuracy [Figs. 4(b) and 5(a)] because of the insufficient number of experimental data for the π^*-conduction band, which is close to the Fermi level. The overlap of both branches of the π^* band induces a large uncertainty on the exact position of this band, noticeably of its energy minimum. This problem might be overcome by

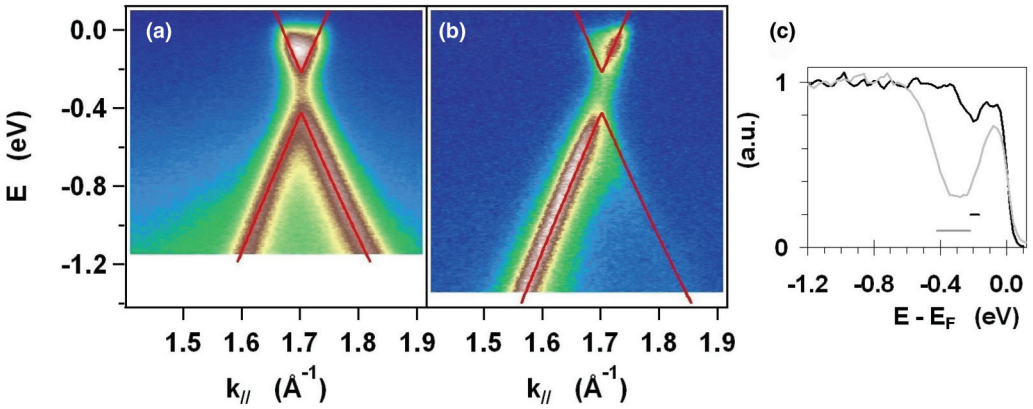

FIG. 5. (Color online) The valence band dispersion measured by ARPES parallel to the ΓK direction (a) $h\nu = 30$ eV, circular polarization, and (b) $h\nu = 100$ eV, linear polarization, for monolayer-MBE graphene grown at 1180 °C on the C face of SiC for graphene domains oriented along the [11-20] SiC direction. The continuous lines (a, b) are the tight-binding best fits. The Fermi level is taken as energy reference. The normalized intensity maximum of the momentum distribution curves vs the binding energy for bilayer (dark line) or monolayer (gray line) graphene are presented in (c), for $h\nu = 100$ eV and linear polarization, with the horizontal lines representing the respective tight-binding fitted positions of the band gap.

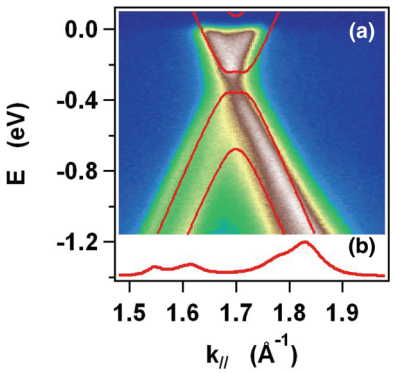

FIG. 6. (Color online) The valence band dispersion measured by ARPES along the ΓK direction for bilayer-MBE graphene grown at 1140 °C on the Si face of SiC, with $h\nu = 30$ eV and circular polarization (a) and momentum distribution curve for $E = -1.1$ eV (b), for graphene domains oriented along the [11-20] SiC direction. The continuous lines (a) are the tight-binding best fits.

simultaneously fitting the ARPES 30 eV [Figs. 4(a), 4(b), and 5(a)] and 100 eV experiments [Figs. 4(c) and 5(b)] for each sample. Only one branch is observed for each band in this last case (the dark corridor effect, see above). To obtain a satisfactory fit, it is mandatory to add an adjustable band gap E_G between the π and π^* bands to the formula (4) presented by Bostwick *et al.*[31] This means that the π and π^* bands are rigidly shifted in opposite directions to obtain an energy band gap of width equal to E_G at the Dirac point. This is obvious in the ML case [Figs. 5(a) and 5(b)], for which a band gap of 200 meV is obtained. In the bilayer case [Figs. 4(a), 4(b), and 4(c)], the best simultaneous fits suggest a 50 meV band gap. The occurrence of a gap is further demonstrated by the ARPES normalized energy distribution curves taken at maximum intensity shown in Fig. 5(c). A clear decrease is observed for ML graphene at the gap position, while a smaller dip closer to the Fermi level is seen for the bilayer sample [see the schematized energy band gap shown by the horizontal lines in Fig. 5(c)].

The occurrence of a band gap is not expected in infinite-size isolated ML graphene. Indeed, graphene might be described as a zero band gap semiconductor because of its 2D structure with two carbon atoms per unit cell, symmetrically located at positions known as A and B. The symmetry between both A and B sublattices is responsible for the graphene band structure and implies the degeneracy of the π and π^* bands at the K and K' Dirac points. Breaking the A-B lattice symmetry implies raising this degeneracy and induces a band gap. Many factors were demonstrated to be able to generate a band gap in graphene, including confinement in reduced-size domains, edge effects, and interaction with the substrate or strain. Graphene electronic field-effect transistor applications have driven many experimental studies of lateral confinement in nanoribbons.[46,47] For example, electronic transport measurements in lithographically patterned structures led to the conclusion that ~20 nm-wide graphene ribbons could induce a ~200 meV band gap.[46] This order of magnitude of the gap is consistent with the ones obtained by *ab initio* calculations.[48,49] These studies concluded that quantum confinement induces a band gap in graphene, the width of which decreases when the ribbon width increases. It also showed that edge effects are crucial for determining the exact gap value.[49] The edge effects were later confirmed to induce a conduction gap in graphene nanoribbons through edge-disorder-induced localization.[50] Although the confinement and edge effects might appear inconsistent with the domain size shown by AFM images in Fig. 3, the AFM lateral resolution might not be sufficient to image the real size of the graphene domains. When graphene stands on a susbtrate, the atomic-stacking structure may result in a band gap. This was shown by *ab initio* calculations for graphene on Boron Nitride (BN), for which the BN-induced A-B lattice asymmetry is responsible for opening a 55 meV band gap.[51] A similar effect was demonstrated by ARPES experiments for graphene on Ni with intercalation of one ML of metallic atoms.[52] Band gaps of 180 meV (respectively 320 meV) were measured for Cu and Ag but none for the Au intercalation. The substrate may also be responsible for a strain-induced band gap; however, the particular strain characteristics required for such an effect[53,54] may be met on flexible substrates but not on the flat SiC used here. The LEED patterns shown in Fig. 2 are indeed consistent with almost strain-free graphene. Recently, it was calculated that preferential incorporation of the N dopant in one particular sublattice would induce a gap in graphene.[55] A similar effect could be efficient for Si as well, although neither calculations nor experiments are yet performed. Because Si is isoelectronic with C, doping effects are not expected in this case. Therefore, if strain may be ruled out, quantum confinement, preferential Si incorporation, and edge and substrate effects may all contribute to the opening of a band gap in the Si-assisted MBE graphene. The reduced energy gap observed in the bilayer sample compared to the ML case suggests that the incomplete graphene layer of the nominally ML sample may be (partially) responsible for the occurrence of a band gap because of confinement and/or irregular edge effects. In fact, the quantum confinement should be reduced if the domain size increases with the graphene thickness. Similarly, edge effects may be lowered at the same time by reducing the edge disorder, which is consistent with the reduction of the defect-related peak intensity measured in Raman spectroscopy (not shown) in the bilayer sample compared to the ML one. However, the gap reduction in the bilayer sample is also consistent with substrate coupling effects, since it was shown that the substrate-induced gap opening and doping are correlated[52] (the reduction of the doping in the bilayer sample is discussed in the next paragraph). Therefore, although their relative contribution may be thickness-dependent, none of the quantum confinement, edge-, or substrate-related mechanisms for opening a band gap in graphene can be excluded at this stage. Complementary studies are obviously required to understand the origin of a gap in the Si-assisted MBE graphene. It must finally be pointed out that the origin of the band gap is completely different in the C- and Si-face samples. In the latter case, it results from the inequivalent charge states of both graphene planes in a Bernal-stacked bilayer structure. This effect was detailed, for example, by Bostwick *et al.*[31] and is also observed by Si-assisted MBE growth [a gap of ~120 meV is deduced from the tight-binding best fitting, see Fig. 6(a)].

The energy position of the Dirac point E_D is less clearly defined when a gap is present. One may nevertheless assume

that it is located at midgap[52] in order to study its thickness dependency and to compare the doping in our Si-assisted MBE graphene samples with the data already published in the literature. The difference $E_F - E_D$ is thus, respectively, 320 meV and 190 meV for ML and bilayer graphene (see Table I). These values agree with some of the previously published experiments.[26,27] Noticeably, differential interband transmission-transient spectroscopic measurements[27] were achieved on a thick sample (63 ML) and were able to associate the level of doping with each individual layer (at least for doping larger than 90 meV, for SiC-transparency reasons). Doping of 360 meV and 215 meV, respectively, were obtained for the highly doped layers one and two, close to the SiC substrate, which quantitatively fit our $E_F - E_D$ ARPES data. Let us remark that the conclusions drawn after such interband experiments do not depend on the occurrence of a band gap. A rather good agreement is also found with k-resolved photoemission electron microscopy experiments,[26] which were able to measure the valence band photoemission from single graphene domains but at the expense of the energy and k-space resolutions. The n-type doping is also consistent with the transport measurements that conclude to electron doping in the first graphene layer.[3,56] On the contrary, our ARPES measurements disagree with the ones published by Johansson *et al.*[25] and to a less critical extent by Hicks *et al.*[23] In the latter study, 3–10-ML-thick graphene was measured by ARPES, showing a low p-type doping (15 meV). Since the samples studied in Refs. 23, 26, and 27 were all obtained from the same growth set-up using the confinement-controlled sublimation of the SiC method in the temperature range 1450–1600 °C,[10] one cannot invoke the growth conditions as being responsible for doping differences. In fact, assuming that the measurements published in Ref. 23 were dominated by the thicker domains is sufficient to raise the doping discrepancy in this latter case. On the contrary, the disagreement with the data published in Ref. 25 is not understood right now. Their spatially unresolved ARPES results lead them to conclude to a low doping below 75 meV (for an average thickness 2 ML) and 50 meV (3 ML), respectively. The corresponding thicknesses were determined thanks to the high spatial resolution low-energy electron microscopy measurements in a separate chamber, making correlation with the ARPES measurements not straightforward. The discrepancy with our measurements may also be a real effect, arising from their graphene fabrication technique that involves very high temperature anneal under an Ar ambient (pressure range 500–850 mbar). Indeed, a significantly higher temperature range (1800–2000 °C) was used in Ref. 25, compared to 1100–1200 °C (MBE, this work) and to 1450–1600 °C,[10] and may be responsible for a reduced doping or coupling with the substrate. It must be also considered that oxygen from unsufficiently purified Ar gas could affect the graphene properties on (000-1) SiC.[57] Indeed, it was reported that the presence of oxygen induces hole doping for exfoliated graphene on SiO_2,[58] leading to electron donor compensation. Further studies are required to understand this discrepancy.

In conclusion, high energy and k-space resolution ARPES experiments were achieved on nominally single and bilayer graphene grown by Si-flux assisted MBE on SiC. These measurements allow us to obtain a unified description of the doping issue in the case of graphene on SiC, at least for growth temperatures up to 1600 °C. The SiC substrate induces a strong doping by charge transfer for both faces, with a Dirac point located 300–450 meV below the Fermi level for ML graphene. In the case of rotationally disordered graphene on (000-1) SiC, the efficient screening by the successive graphene layers reduces the doping, as was previously concluded after differential interband transmission spectroscopy[27] and directly confirmed by ARPES in this work. This agreement emphasizes the potentialities of the Si-flux assisted MBE technique, more particularly for homogeneous low-thickness graphene growth on (000-1) SiC. The observation of the thickness-dependent doping and energy band gap by nonspatially resolved ARPES measurements is strongly encouraging in this respect.

ACKNOWLEDGMENTS

This work has been achieved with the financial support of the French ANR (Project Xp-Graphene), the Nord-Pas de Calais Regional Council, the European Commission (project GRADE), and the RENATECH network.

*Corresponding author: dominique.vignaud@univ-lille1.fr

[1] A. J. Van Bommel, J. E. Crombeen, and A. Van Tooren, Surf. Sci. **48**, 463 (1975).

[2] C. Berger, Z. Song, T. Li, X. Li, A. Y. Ogbazghi, R. Feng, Z. Dai, A. N. Marchenkov, E. H. Conrad, P. N. First, and W. A. de Heer, J. Phys. Chem. B **108**, 19912 (2004).

[3] C. Berger, Z. Song, X. Li, X. Wu, N. Brown, C. Naud, D. Mayou, T. Li, J. Hass, A. N. Marchenkov, E. H. Conrad, P. N. First, and W. A. de Heer, Science **312**, 1191 (2006).

[4] J. Hass, W. A. de Heer, and E. H. Conrad, J. Phys.: Condens. Matter **20**, 323202 (2008).

[5] K. V. Emtsev, F. Speck, T. Seyller, L. Ley, and J. D. Riley, Phys. Rev. B **77**, 155303 (2008).

[6] L. Magaud, F. Hiebel, F. Varchon, P. Mallet, and J. Y. Veuillen, Phys. Rev. B **79**, 161405 (2009).

[7] C. Faugeras, A. Nerrière, M. Potemski, A. Mahmood, E. Dujardin, C. Berger, and W. A. de Heer, Appl. Phys. Lett. **92**, 011914 (2008).

[8] J. Hass, F. Varchon, J. E. Millan-Otoya, M. Sprinkle, N. Sharma, W. A. de Heer, C. Berger, P. N. First, L. Magaud, and E. H. Conrad, Phys. Rev. Lett. **100**, 125504 (2008).

[9] C. Virojanadara, M. Syväjarvi, R. Yakimova, L. I. Johansson, A. A. Zakharov, and T. Balasubramanian, Phys. Rev. B **78**, 245403 (2008).

[10] W. A. de Heer, C. Berger, M. Ruan, M. Sprinkle, X. Li, Y. Hu, B. Zhang, J. Hankinson, and E. H. Conrad, Proc. Natl. Acad. Sci. **108**, 16900 (2011).

[11] A. Al-Temimy, C. Riedl, and U. Starke, Appl. Phys. Lett. **95**, 231907 (2009).

[12] E. Moreau, F. J. Ferrer, D. Vignaud, S. Godey, and X. Wallart, Phys. Status Solidi A **207**, 300 (2010).

[13]E. Moreau, F. J. Ferrer, D. Vignaud, S. Godey, X. Wallart, J. Avila, M. C. Asensio, F. Bournel, and J. J. Gallet, Appl. Phys. Lett. **97**, 241907 (2010)
[14]J. Hwang, V. B. Shields, C. I. Thomas, S. Shivaraman, D. Hao, M. Kim, A. R. Woll, G. S. Tompa, and M. G. Spencer, J. Cryst. Growth **312**, 3219 (2010).
[15]W. Strupinski, K. Grodecki, A. Wysmolek, R. Stepniewski, T. Szkopek, P. E. Gaskell, A. Grüneis, D. Haberer, R. Bozek, J. Krupka, and J. M. Baranowsli, Nano Lett. **11**, 1786 (2011).
[16]A. H. Castro-Neto, F. Guinea, N. M. R. Peres, K. S. Novoselov, and A. K. Geim, Rev. Mod. Phys. **81**, 109 (2009).
[17]J. Ristein, S. Mammadov, and T. Seyller, Phys. Rev. Lett. **108**, 246104 (2012).
[18]T. Ohta, A. Bostwick, T. Seyller, K. Horn, and E. Rotenberg, Science **313**, 951 (2006).
[19]T. Ohta, A. Bostwick, J. L. McChesney, T. Seyller, K. Horn, and E. Rotenberg, Phys. Rev. Lett. **98**, 206802 (2007).
[20]A. Bostwick, T. Ohta, T. Seyller, K. Horn, and E. Rotenberg, Nature Phys. **3**, 36 (2007).
[21]S. Y. Zhou, D. A. Siegel, A. V. Fedorov, and A. Lanzara, Phys. Rev. Lett. **101**, 086402 (2008).
[22]I. Gierz, J. Henk, H. Höchst, C. R. Ast, and K. Kern, Phys. Rev. B **83**, 121408 (2011).
[23]J. Hicks, M. Sprinkle, K. Shepperd, F. Wang, A. Tejeda, A. Taleb-Ibrahimi, F. Bertran, P. Le Fèvre, W. A. de Heer, C. Berger, and E. H. Conrad, Phys. Rev. B **83**, 205403 (2011).
[24]M. Sprinkle, D. Siegel, Y. Hu, J. Hicks, A. Tejeda, A. Taleb-Ibrahimi, P. Le Fèvre, F. Bertran, S. Vizzini, H. Enriquez, S. Chiang, P. Soukiassian, C. Berger, W. A. de Heer, A. Lanzara, and E. H. Conrad, Phys. Rev. Lett. **103**, 226803 (2009).
[25]L. I. Johansson, S. Watcharinyanon, A. A. Zakharov, T. Iakimov, R. Yakimova, and C. Virojanadara, Phys. Rev. B **84**, 125405 (2011).
[26]C. Mathieu, N. Barrett, J. Rault, Y. Y. Mi, B. Zhang, W. A. de Heer, C. Berger, E. H. Conrad, and O. Renault, Phys. Rev. B **83**, 235436 (2011).
[27]D. Sun, C. Divin, C. Berger, W. A. de Heer, P. N. First, and T. B. Norris, Phys. Rev. Lett. **104**, 136802 (2010).
[28]Y. J. Song, A. F. Otte, Y. Kuk, Y. Hu, D. B. Torrance, P. N. First, W. A. de Heer, H. Min, S. Adam, M. D. Stiles, A. H. MacDonald, and J. A. Stroscio, Nature **467**, 185 (2010).
[29]D. L. Miller, K. D. Kubista, G. M. Rutter, M. Ruan, W. A. de Heer, P. N. First, and J. A. Stroscio, Science **324**, 924 (2009).
[30]M. A. Kuroda, J. Tersoff, and G. J. Martyna, Phys. Rev. Lett. **106**, 116804 (2011).
[31]A. Bostwick, J. McChesney, T. Ohta, E. Rotenberg, T. Seyller, and K. Horn, Prog. Surf. Sci. **84**, 380 (2009).
[32]I. Crassee, J. Levallois, D. van der Marel, A. L. Walter, T. Seyller, and A. B. Kuzmenko, Phys. Rev. B **84**, 035103 (2011).
[33]A. Sidorov, K. Gaskill, M. B. Nardelli, J. L. Tedesco, R. L. Myers-Ward, C. R. Eddy, T. Jayasekera, H. K. W. Kim, R. Jayasingha, A. Sherehiy, R. Stallard, and G. U. Sumanasekera, J. Appl. Phys. **111**, 013706 (2012).
[34]J. Hass, R. Feng, J. E. Millan-Otoya, X. Li, M. Sprinkle, P. N. First, W. A. de Heer, E. H. Conrad, and C. Berger, Phys. Rev. B **75**, 214109 (2007).
[35]X. Wu, Y. Hu, M. Ruan, N. K. Madiomanana, J. Hankinson, M. Sprinkle, C. Berger, and W. A. de Heer, Appl. Phys. Lett. **95**, 223108 (2009).
[36]E. Moreau, Ph.D. Thesis, University of Lille, 2011; http://tel.archives-ouvertes.fr/tel-00665851.
[37]F. J. Ferrer, E. Moreau, D. Vignaud, S. Godey, and X. Wallart, Semicond. Sci. Technol. **24**, 125014 (2009).
[38]L. B. Biedermann, M. L. Bolen, M. A. Capano, D. Zemlyanov, and R. G. Reifenberger, Phys. Rev. B **79**, 125411 (2009).
[39]F. J. Ferrer, E. Moreau, D. Vignaud, D. Deresmes, S. Godey, and X. Wallart, J. Appl. Phys. **109**, 054307 (2011).
[40]E. L. Shirley, L. J. Terminello, A. Santoni, and F. J. Himpsel, Phys. Rev. B **51**, 13614 (1995).
[41]C. Riedl, Ph.D. Thesis, University of Erlangen-Nürnberg, 2010; www.opus.ub.uni-erlangen.de/opus/volltexte/2010/1992/pdf/ChristianRiedlDissertation.pdf.
[42]F. Hiebel, L. Magaud, P. Mallet, and J. Y. Veuillen, J. Phys. D: Appl. Phys. **45**, 154003 (2012).
[43]M. L. Bolen, S. E. Harrison, L. B. Biedermann, and M. A. Capano, Phys. Rev. B. **80**, 115433 (2009).
[44]K. R. Knox, S. Wang, A. Morgante, D. Cvetko, A. Locatelli, T. O. Mentes, M. A. Nino, P. Kim, and R. M. Osgood, Phys. Rev. B **78**, 201408 (2008).
[45]M. Mucha-Kruczynski, O. Tsyplyatyev, A. Grishin, E. McCann, V. I. Fal'ko, A. Bostwick, and E. Rotenberg, Phys. Rev. B **77**, 195403 (2008).
[46]M. Y. Han, B. Ozyilmaz, Y. Zhang, and P. Kim, Phys. Rev. Lett. **98**, 206805 (2007).
[47]Z. Chen, Y. M. Lin, M. J. Rooks, and P. Avouris, Physica E **40**, 228 (2007).
[48]V. Barone, O. Hod, and G. E. Scuseria, Nano Lett. **6**, 2748 (2006).
[49]Y. W. Son, M. L. Cohen, and S. G. Louie, Phys. Rev. Lett. **97**, 216803 (2006).
[50]M. Evaldsson, I. V. Zozoulenko, H. Xu, and T. Heinzel, Phys. Rev. B **78**, 161407 (2008).
[51]G. Giovannetti, P. A. Khomyakov, G. Brocks, P. J. Kelly, and J. van den Brink, Phys. Rev. B **76**, 073103 (2007).
[52]A. Varykhalov, M. R. Scholz, T. K. Kim, and O. Rader, Phys. Rev. B **82**, 121101 (2010).
[53]V. M. Pereira, A. H. CastroNeto, and N. M. R. Peres, Phys. Rev. B **80**, 045401 (2009).
[54]G. Cocco, E. Caledano, and L. Colombo, Phys. Rev. B **81**, 241412(R) (2010).
[55]A. Lherbier, A. R. Botello-Méndez, and J. C. Charlier, Nano Lett. **13**, 1446 (2013).
[56]W. A. de Heer, C. Berger, X. Wu, P. N. First, E. H. Conrad, X. Li, T. Li, M. Sprinkle, J. Hass, M. L. Sadowski, M. Potemski, and G. Martinez, Solid State Commun. **143**, 92 (2007).
[57]Luxmi, N. Srivastava, G. He, R. M. Feenstra, and P. J. Fisher, Phys. Rev. B **82**, 235406 (2010).
[58]S. Ryu, L. Liu, S. Berciaud, Y. J. Yu, H. Liu, P. Kim, G. W. Flynn, and L. E. Brus, Nano Lett. **10**, 4944 (2010).